Organic Electronics 97 (2021) 106275

Contents lists available at ScienceDirect

Organic Electronics

journal homepage: www.elsevier.com/locate/orgel

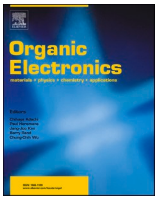

A periphery cladding strategy to improve the performance of narrowband emitters, achieving deep-blue OLEDs with $CIE_y < 0.08$ and external quantum efficiency approaching 20%

Yaxiong Wang, Yalei Duan, Runda Guo **, Shaofeng Ye, Kaiyuan Di, Weizhuo Zhang, Shaoqing Zhuang, Lei Wang *

Wuhan National Laboratory for Optoelectronics, Huazhong University of Science and Technology, Wuhan, 430074, People's Republic of China

ARTICLE INFO

Keywords:
Thermally activated delayed fluorescence
Deep-blue emission
Boron derivatives
Multiple resonance effects
OLEDs

ABSTRACT

Deep-blue thermally activated delayed fluorescence (TADF) emitters with National Television System Committee (NTSC) standard (0.14, 0.08) and narrowband emission have been one of the challenging issues for organic light-emitting diodes (OLEDs). In this work, a novel molecular design strategy, periphery cladding, was used to design and synthesize three deep-blue multi-resonance TADF emitters, N,N, 5,9-tetraphenyl-5,9-dihydro-5,9-diaza-13b-boranaphtho[3,2,1-*de*]anthracen-7-amine (**PAB**), 2,12-di-*tert*-butyl-5,9-bis(4-(*tert*-butyl)phenyl)-*N,N*-diphenyl-5,9-dihydro-5,9-diaza-13b-boranaphtho[3,2,1-*de*]anthracen-7-amine (**2tPAB**) and 2,12-di-*tert*-butyl-N,N,5,9-tetrakis(4-(*tert*-butyl)phenyl)-5,9-dihydro-5,9-diaza-13b-boranaphtho[3,2,1-*de*]anthracen-7-amine (**3tPAB**). By cladding large steric hindrance *tert*-butyl unit at periphery of multi-resonance emitter, the intermolecular interactions were suppressed, thus reducing aggregation-induced emission quenching and improving the PLQY of emitter. **3tPAB** with full periphery cladding exhibited higher PLQY (74.7%). As a result, the device based on **3tPAB** acquired the best performance by using 1,3-di(9*H*-carbazol-9-yl)benzene (mCP) with low polarity as host. The maximum external quantum efficiency (EQE_{max}), CIE coordinates, and full-width at half-maximum (FWHM) of **3tPAB**-based device were 19.3%, (0.141, 0.076), and 26 nm, respectively. To our knowledge, this is the first report about narrowband TADF OLEDs with single host that EQE_{max} approaches 20% while CIE coordinates meet the NTSC blue-light standard.

1. Introduction

Organic-light-emitting diodes (OLEDs) have been used in the field of intelligent display owing to the high contrast ratio and rapid response time [1–7]. The conventional organic luminescent material such as conventional fluorescent, phosphorescent, and thermally activated delayed fluorescence (TADF) emitters with the donor (D)-acceptor (A) structure exhibits strong vibronic coupling between the ground state (S_0) and singlet excited state (S_1) as well as structural relaxation at the S_1 state, leading to broad emission bands with full-width at half-maximum (FWHM) of >40 nm [8–14]. Therefore, to satisfy the requirement of high resolution and wide color gamut for new-generation display, the device usually employs color filters and/or optical microcavities technologies to enhance color purity. However, these technologies will increase the cost of the fabrication process, impeding the practical applications of OLEDs [15]. Recently, the novel TADF emitters based on multiple resonance effects have aroused the wide concern of researchers because of the high efficiency and narrowband emission [16,17]. These series of materials allow the lowest unoccupied molecular orbitals (LUMO) and the highest occupied molecular orbitals (HOMO) to be distributed on different atoms, thus minimizing their bonding/antibonding character, decreasing the vibronic coupling and vibrational relaxation of material. The FWHM can reach 14 nm, showing a great promising application [18].

At present, full-Color TADF emitters with narrowband emission have been achieved. The external quantum efficiency of blue-, green-, and red-light narrowband TADF-based OLEDs have realized 34.4% [18], 31.8% [19], and 22.0% [19], respectively. However, the deep-blue narrowband TADF-based OLEDs that can match the National Television System Committee (NTSC) standard (0.14, 0.08) have not been

---

* Corresponding author.
** Corresponding author.
E-mail addresses: runda_guo@hust.edu.cn (R. Guo), wanglei@mail.hust.edu.cn (L. Wang).

https://doi.org/10.1016/j.orgel.2021.106275
Received 18 June 2021; Received in revised form 24 June 2021; Accepted 24 June 2021

reported [17,20–23]. To achieve this goal, molecular engineering and device engineering need a reasonable combination. From molecular design, multiple resonance core for narrowband TADF emission can be classified as a fused nitrogen/carbonyl (N/C$=$O) system and a fused boron/nitrogen (B/N) system [24–34]. Compared with the fused N/C$=$O system, the fused B/N system exhibits much more multiple structural modifiability, arousing more attention. According to the most recent findings of the fused B/N system, the para-disposed two boron atoms (B-π-B) and para-disposed two nitrogen atoms (N-π-N) in the central π-core will significantly increase the acceptor and donor strengths, resulting in large bathochromic shifts of emission. Nevertheless, para-disposed boron and nitrogen atoms (B-π-N) can reduce the acceptor and donor strengths, thus realizing a shorter-wavelength emission [19]. As a result, a fused B/N system with a B-π-N structure is possible for deep-blue emission. Simultaneously, the limited π-conjugation of fused B/N system is also needed [27,28]. Moreover, the TADF emitters suffer from aggregation-induced emission quenching and exciton annihilation processes. The substituents with large steric hindrance such as *tert*-butyl unit are necessary to suppress the negative effect, thus enhancing luminous efficiency [35–37]. From device engineering, most narrowband TADF-based OLEDs employ bipolar material as host can improve device efficiency [27–30]. However, the strong polarity of host will give rise to the interactions between hosts and emitters, shifting electroluminescence spectra to long-wavelength. Therefore, it is anticipated that high efficiency and deep-blue emission can be obtained by cladding large steric hindrance *tert*-butyl unit at periphery of multi-resonance emitter with B-π-N structure and selecting the low polarity host.

In this work, N,N,5,9-tetraphenyl-5,9-dihydro-5,9-diaza-13b-boranaphtho[3,2,1-de]anthracen-7-amine (**PAB**) with B-π-N structure was designed as a parent molecule. By partial and full periphery cladding with *tert*-butyl unit, 2,12-di-*tert*-butyl-5,9-bis(4-(*tert*-butyl)phenyl)-*N*,*N*-diphenyl-5,9-dihydro-5,9-diaza-13b-boranaphtho[3,2,1-de]anthracen-7-amine (**2tPAB**) and 2,12-di-*tert*-butyl-N,N,5,9-tetrakis(4-(*tert*-butyl)phenyl)-5,9-dihydro-5,9-diaza-13b-boranaphtho[3,2,1-de] anthracen-7-amine (**3tPAB**) were further synthesized. The results showed all new emitters with B-π-N structure exhibited deep-blue narrowband TADF emission with peak at 449–456 nm and FHWM of 23–26 nm in toluene solution. Under the periphery cladding of *tert*-butyl units, the intermolecular interactions were suppressed, and the PLQY of emitter was enhanced. However, the singlet-triplet splitting (ΔE_{ST}) was increased, which reduced reverse intersystem crossing rate constant (k_{RISC}). By using 1,3-di(9*H*-carbazol-9-yl)benzene (mCP) with low polarity as host, **3tPAB**-based device achieved the best performance with the maximum external quantum efficiency (EQE_{max}) of 19.3% and CIE coordinates of (0.141, 0.076), respectively. To our knowledge, this is the first report about narrowband TADF OLEDs with single host that EQE_{max} approached 20% while CIE coordinates met the NTSC blue-light standard.

2. Experimental section

2.1. Materials and reagents

All the solvents and reagents used for target compounds were purchased from commercial suppliers without further purification.

2.2. Synthesis

N^1,N^1,N^3,N^3,N^5,N^5-hexaphenylbenzene-1,3,5-triamine (***PA***): The mixture of 1,3,5-tribromobenzene (4.00 g, 12.7 mmol), diphenylamine (6.70 g, 39.40 mmol), $Pd_2(dba)_3$ (0.17 g, 0.19 mmol), $P(t\text{-}Bu)_3{\cdot}HBF_4$ (0.13 g, 0.44 mmol) and NaOt-Bu (3.66 g, 38.1 mmol) was suspended in toluene (60 mL) and refluxed for 18 h under N_2 atmosphere at 120 °C. The reaction mixture was cooled to room temperature, toluene was removed by vacuum distillation. Then the crude product was extracted by dichloromethane and water. The organic layer was dried by $MgSO_4$, then filtered and concentrated in vacuo. Finally, the residue was purified by column chromatography (elution solvent: petroleum ether) to afford a white solid (6.42g). Yield, 86%. ^{1}H NMR (400 MHz, $CDCl_3$) δ [ppm]: δ 7.16 (t, J = 7.8 Hz, 12H), 7.07–6.98 (m, 12H), 6.91 (t, J = 7.3 Hz, 6H), 6.42 (s, 3H).

3,5-dichloro-N,N-diphenylaniline (***PA*-2Cl**): The synthetic procedure was similar to that of **PA**. White solid was obtained. Yield, 83%. ^{1}H NMR (400 MHz, $CDCl_3$) δ [ppm]: δ 7.31 (t, J = 7.8 Hz, 4H), 7.11 (t, J = 8.8 Hz, 6H), 6.87 (dd, J = 11.7, 1.5 Hz, 3H).

N^1,N^1,N^3,N^3-tetrakis(4-(tert-butyl)phenyl)-N^5,N^5-diphenylbenzene-1,3,5-triamine (***2tPA***): The mixture of 1,3,5-tribromobenzene (4.50 g, 14.3 mmol), bis(4-(*tert*-butyl)phenyl)amine (8.46 g, 30.06 mmol), $Pd_2(dba)_3$ (0.065 g, 0.072 mmol), $P(t\text{-}Bu)_3$ (10 wt% in toluene, 0.35 mL, 0.143 mmol) and NaOt-Bu (5.49 g, 57.2 mmol) was suspended in toluene (70 mL) and refluxed for 18 h under N_2 atmosphere at 120 °C. The reaction mixture was cooled to room temperature, toluene was removed by vacuum distillation. Then the crude product was extracted by dichloromethane and water. The organic layer was dried by $MgSO_4$, then filtered and concentrated in vacuo. Finally, the residue was purified by column chromatography (elution solvent: petroleum ether then petroleum ether/dichloromethane = 9:1) to afford a white solid (6.62g). Yield, 57%. ^{1}H NMR (400 MHz, $CDCl_3$) δ [ppm]: δ 7.14 (dd, J = 14.4, 8.0 Hz, 12H), 7.02 (d, J = 7.7 Hz, 4H), 6.96 (d, J = 8.6 Hz, 8H), 6.88 (t, J = 7.3 Hz, 2H), 6.55 (s, 1H), 6.29 (d, J = 1.8 Hz, 2H), 1.37–1.19 (m, 36H).

N^1,N^1,N^3,N^3,N^5,N^5-hexakis(4-(tert-butyl)phenyl)benzene-1,3,5-triamine (***3tPA***): The synthetic procedure was similar to that of **PA**. White solid was obtained. Yield, 91%. ^{1}H NMR (400 MHz, $CDCl_3$) δ [ppm]: δ 7.17 (t, J = 10.4 Hz, 12H), 6.95 (d, J = 8.5 Hz, 12H), 6.44 (s, 3H), 1.26 (s, 54H).

N,N,5,9-tetraphenyl-5,9-dihydro-5,9-diaza-13b-boranaphtho[3,2,1-de] anthracen-7-amine (***PAB***): Boron tribromide (3.19 mL, 33.1 mmol) was added to a solution of **PA** (3.21 g, 3.5 mmol) in *o*-dichlorobenzene (100 mL) at room temperature under a nitrogen atmosphere. After stirring at 180 °C for 20 h, the reaction mixture was allowed to cool to 0 °C. After addition of *N*, *N*-diisopropylethylamine (20.5 mL, 124.2 mmol), the solvent was removed in vacuo. The crude product was washed with acetonitrile and recrystallized by toluene and acetonitrile to afford a yellow solid (3.55g). Yield, 73%. ^{1}H NMR (400 MHz, $CDCl_3$) δ [ppm]: δ 8.90 (dd, J = 7.7, 1.4 Hz, 2H), 7.48 (dd, J = 17.1, 9.7 Hz, 4H), 7.37 (ddd, J = 8.6, 5.0, 1.9 Hz, 4H), 7.27–7.17 (m, 6H), 7.08 (dd, J = 10.2, 5.5 Hz, 4H), 6.97–6.86 (m, 6H), 6.71 (d, J = 8.4 Hz, 2H), 5.61 (s, 2H). ^{13}C NMR (101 MHz, $CDCl_3$) δ [ppm]: δ 146.65, 142.17, 134.84, 130.66, 130.35, 130.13, 128.78, 128.09, 125.62, 123.49, 116.83. FTMS (APCI): calculated for $C_{42}H_{30}BN_3$, 587.5330; found, 588.2595.

2,12-di-tert-butyl-5,9-bis(4-(tert-butyl)phenyl)-N,N-diphenyl-5,9-dihydro-5,9-diaza-13b-boranaphtho[3,2,1-de]anthracen-7-amine (**2tPAB**): The synthetic procedure was similar to that of **PAB**. Yellow solid was obtained. Yield, 61%. ^{1}H NMR (400 MHz, $CDCl_3$) δ [ppm]: δ 8.96 (d, J = 2.4 Hz, 2H), 7.46 (dd, J = 8.7, 3.4 Hz, 6H), 7.13 (d, J = 8.5 Hz, 4H), 7.10–7.02 (m, 4H), 6.99–6.85 (m, 6H), 6.76 (d, J = 9.0 Hz, 2H), 5.47 (s, 2H), 1.47 (s, 18H), 1.33 (s, 18H). ^{13}C NMR (101 MHz, $CDCl_3$) δ [ppm]: δ 150.91, 147.97, 146.59, 145.88, 141.46, 139.45, 130.78, 129.50, 128.66, 127.92, 127.37, 125.94, 123.49, 116.52, 34.65, 34.32, 31.76, 31.42. FTMS (APCI): calculated for $C_{58}H_{62}BN_3$, 811.9650; found, 812.5106.

2,12-di-tert-butyl-N,N,5,9-tetrakis(4-(tert-butyl)phenyl)-5,9-dihydro-5,9-diaza-13b-boranaphtho[3,2,1-de]anthracen-7-amine (**3tPAB**): The synthetic procedure was similar to that of **PAB**. After recrystallization, the crude product was purified by column chromatography (elution solvent: petroleum ether). Yellow solid was obtained. Yield, 30%. ^{1}H NMR (400 MHz, $CDCl_3$) δ [ppm]: δ 8.93 (d, J = 2.4 Hz, 2H), 7.49–7.42 (m, 6H), 7.15 (d, J = 8.5 Hz, 4H), 7.07 (t, J = 5.7 Hz, 4H), 6.86–6.80 (m, 4H), 6.63 (d, J = 9.0 Hz, 2H), 5.70 (s, 2H), 1.46 (s, 18H), 1.33 (s, 18H), 1.27 (s, 18H). ^{13}C NMR (101 MHz, $CDCl_3$) δ [ppm]: δ 151.00, 147.78,

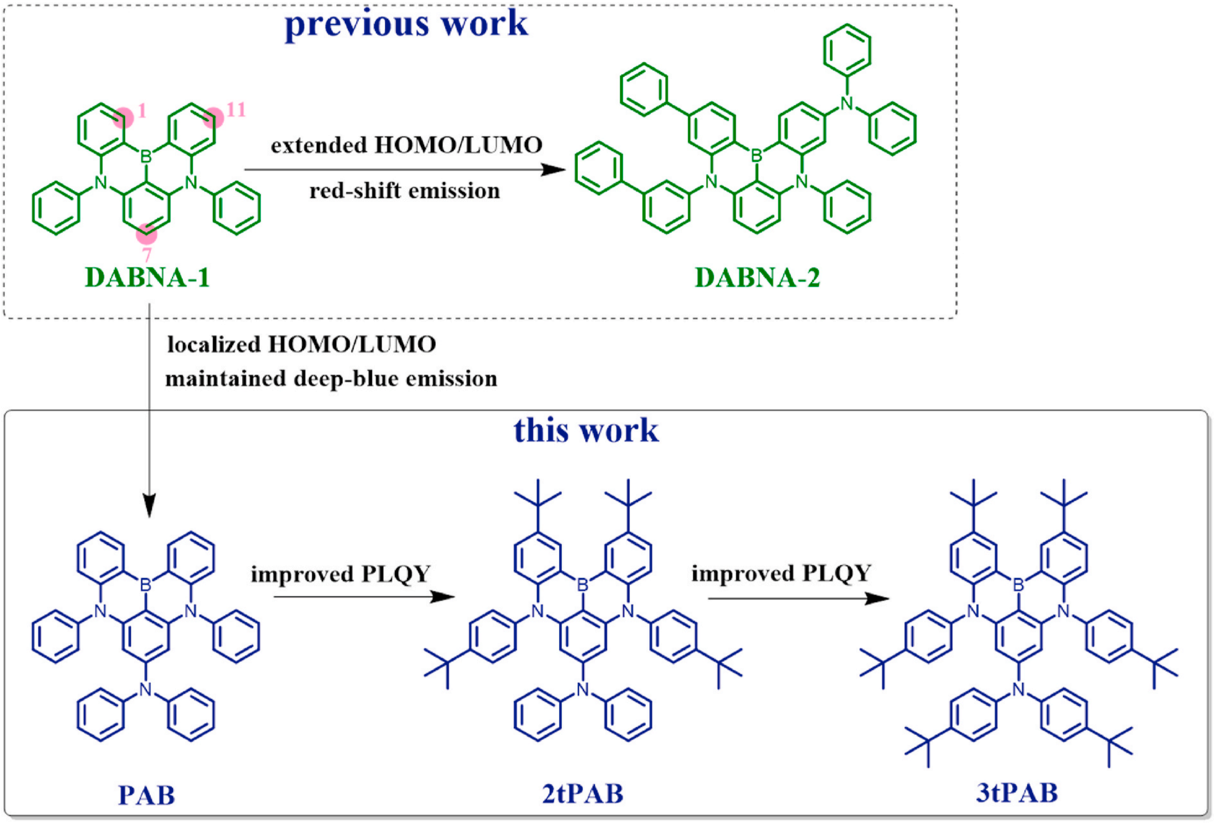

Fig. 1. The design diagram of emitters in previous [38] and this work.

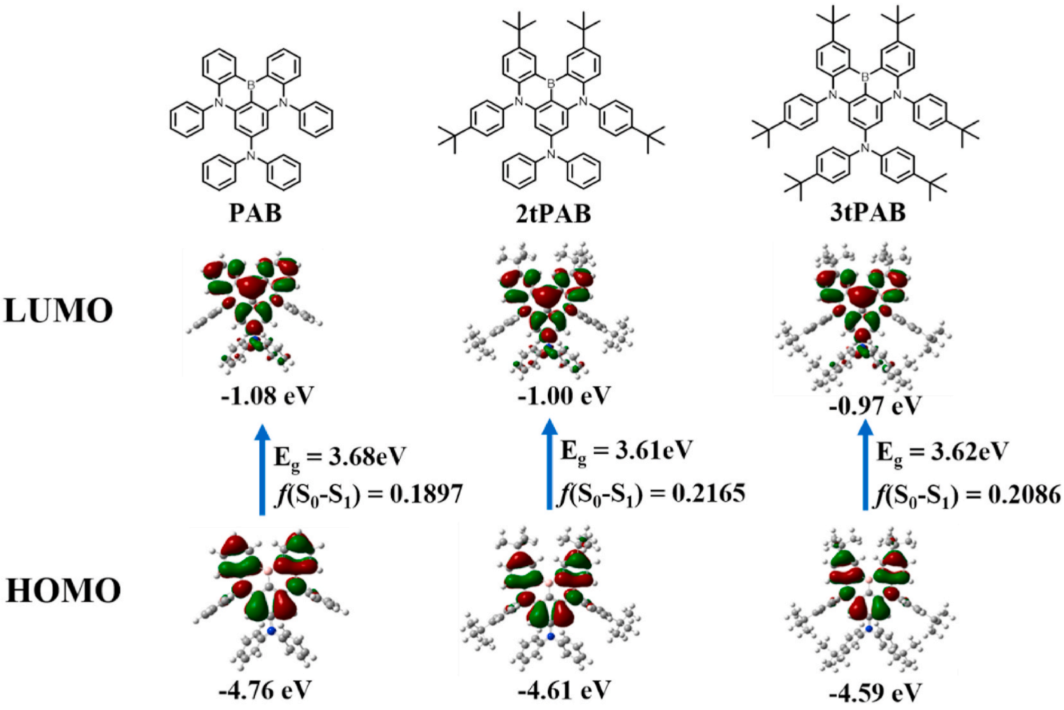

Fig. 2. Distributions of frontier molecular orbitals of **PAB**, **2tPAB**, and **3tPAB**.

146.11, 145.36, 144.48, 141.49, 139.43, 130.81, 129.59, 127.97, 127.33, 125.28, 123.99, 116.51, 99.99, 99.73, 34.68, 34.31, 34.17, 31.75, 31.49, 31.44. FTMS (APCI): calculated for $C_{66}H_{78}BN_3$, 924.1810; found, 924.6354.

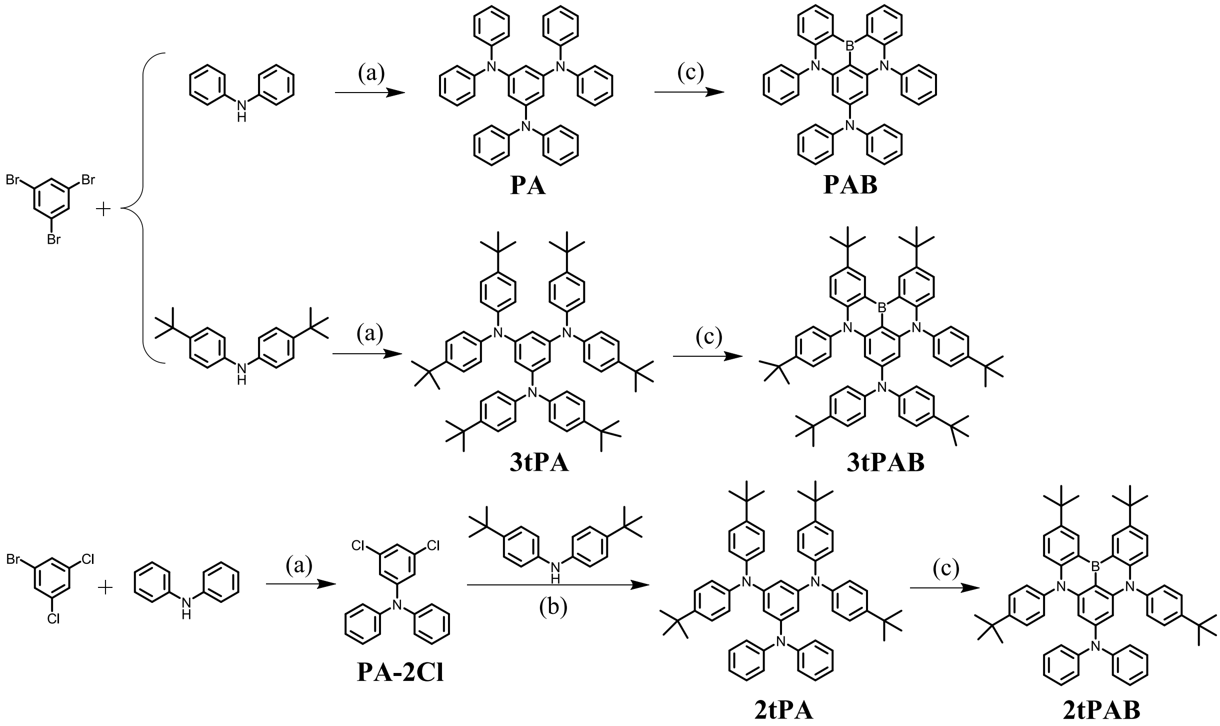

Scheme 1. Synthetic Routes: (a) $Pd_2(dba)_3$, $P(t\text{-}Bu)_3{\cdot}HBF_4$, NaOt-Bu, Toluene, 120 °C, 18h, N_2; (b) $Pd_2(dba)_3$, $P(t\text{-}Bu)_3$, NaOt-Bu, Toluene, 120 °C, 18h, N_2; (c) BBr_3, DIPEA, 180 °C, 20h, N_2.

3. Results and discussion

3.1. Design and synthesis

The parent molecule, **PAB**, was derived from compound DABNA-1 which exhibited deep-blue emission (Fig. 1) [38]. In the previous report, the diphenylamine group was appended onto the asymmetrical position of DABNA-1, i.e. the para-position relative to boron atom (11-position), affording DABNA-2 [38]. However, the LUMO and HOMO distributions of DABNA-2 were extended to the diphenylamine unit, leading to a reduced energy gap (E_g) and the red-shift of emission. Given the impact that the introduction of substituents in asymmetric positions of DABNA-1 will result in the asymmetry of electron-induced effect, further giving rise to the extension of HOMO/LUMO distribution and the red-shift of emission. In this work, the diphenylamine group was attached to the symmetrical position of DABNA-1, i.e. the para-position of boron atom (7-position), to develop **PAB**. Compared with DABNA-1, the LUMO and HOMO distributions of **PAB** were still localized on DABNA-1(Fig. 2). Therefore, deep-blue emission and multiple resonance effects were expected to be maintained. Besides, the introduction of the diphenylamine group will also help to increase the charge-transporting ability of the luminous, improving the performance of the device. Furthermore, **2tPAB** and **3tPAB** were further designed by cladding large steric hindrance *tert*-butyl unit at the periphery of **PAB**. Here, from aggregated states of multiple molecules, a large steric hindrance *tert*-butyl unit can suppress aggregation-induced emission quenching, further enhancing PLQY and improving the luminescence performance.

The synthetic routes of **PAB**, **2tPAB**, and **3tPAB** were shown in Scheme 1. The intermediate compounds (PA, 3tPA, PA-2Cl, and 2tPA) were synthesized by using aromatic nucleophilic substitution and palladium-catalyzed Buchwald-Hartwig reaction. The target compounds were obtained by a one-shot electrophilic arene borylation reaction at 180 °C in nitrogen atmosphere. The details of the preparation and structural characterizations were provided in the experiment section. And all new compounds were unambiguously characterized by nuclear magnetic resonance (NMR) spectroscopy and mass spectroscopy analysis.

Table 1
Photophysical, electrochemical, and thermal analysis data of **PAB**, **2tPAB**, and **3tPAB**.

Compound	T_g/T_d[a] (°C)	λ_{abs}[b] (nm) solution	λ_{em} (nm) solution[b]/film[c]	HOMO[d]/LUMO[e] (eV)	E_S/E_T[f] (eV)	Φ[g] (%)	τ_{PF}[h] (ns)	τ_{DF}[h] (μs)	FWHM[i] (nm)
PAB	NA/372	432	449/453	−5.21/-2.44	2.77/2.71	60.8	7.9	55.7	23
2tPAB	NA/392	436	456/457	−5.08/-2.34	2.76/2.68	67.3	8.1	76.6	26
3tPAB	NA/374	438	456/458	−5.09/-2.36	2.78/2.68	74.7	7.2	74.2	23

[a] T_d was measured by TGA (corresponding to 5% weight loss) and T_g was measured by DSC.

[b] The peak wavelength of the lowest-energy absorption band and the peak wavelength of the PL spectrum in toluene.

[c] The PL peak wavelength in mCP film.

[d] HOMO was estimated from the CV.

[e] LUMO = HOMO + E_{opt}^{g}.

[f] Calculated from the onset of fluorescence (Fl, 77 K) and the phosphorescence (Phos, 77 K) spectra.

[g] Absolute photoluminescence quantum yields.

[h] Lifetime calculated from fluorescence decay and lifetime calculated from delayed fluorescence in the doped film of the emitter in mCP (3 wt%).

[i] Full width at half maximum in toluene.

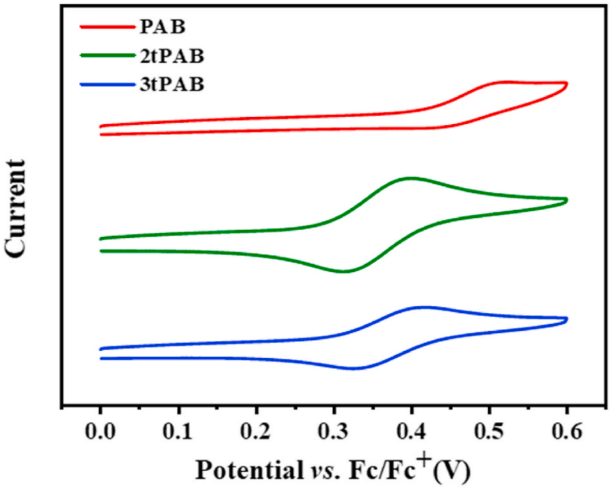

Fig. 3. Cyclic voltammogram of **PAB**, **2tPAB** and **3tPAB**.

3.2. Theoretical calculations

To understand the effect of peripheral cladding *tert*-butyl units on optoelectronic properties of emitters, quantum chemical calculations were performed by using density functional theory (DFT) at the B3LYP/6-31G(d) levels. As shown in Fig. 2, the introduction of peripheral *tert*-butyl units did not affect the distributions of frontier molecular orbitals. The LUMO and HOMO distributions of **PAB**, **2tPAB**, and **3tPAB** were all focused on the DABNA-1 skeleton. Additionally, the LUMOs were localized on the boron atom as well as its ortho/para positions while the HOMOs were localized on the nitrogen atoms as well as its ortho/para positions [38]. The HOMOs and LUMOs were separated at the atomic scale by the multiple resonance effect of the boron and nitrogen atoms. The calculated E_g of **PAB**, **2tPAB**, and **3tPAB** were 3.68, 3.61, and 3.62 eV, respectively. **PAB** without peripheral *tert*-butyl units presented a little higher E_g than **2tPAB**, **3tPAB** and DABNA-1 (E_g, 3.66 eV), which suggested **PAB** would present more blue emission than **2tPAB**, **3tPAB**, and DABNA-1 [38]. The calculated oscillator strengths $f(S_0–S_1)$ of **PAB**, **2tPAB**, and **3tPAB** were 0.1897, 0.2165, and 0.2086, respectively. It was found that **2tPAB**, and **3tPAB** showed higher $f(S_0–S_1)$ than **PAB**. This might be attributed to that large steric hindrance *tert*-butyl substituent suppressed the non-radiative deactivation process, enhancing the $f(S_0–S_1)$.

3.3. Thermal and electrochemical properties

The thermal stabilities of **PAB**, **2tPAB**, and **3tPAB** were measured by thermogravimetric analysis (TGA) and differential scanning calorimetry (DSC) under a nitrogen atmosphere. As shown in Fig. S1 and Table 1, these compounds presented excellent thermal stabilities (Fig. S1), the decomposition temperatures (T_d, corresponding to 5% weight loss) of emitters were around 372–392 °C. However, glass-transition temperatures (T_g) of the three compounds were not observed in the range of 40–300 °C. Such good thermal stability was favorable for OLEDs stability. The electrochemical properties were investigated by cyclic voltammetry (CV) measurement using a traditional three-electrode system (Fig. 3). From the onsets of oxidation potentials, the HOMO energy levels of **PAB**, **2tPAB,** and **3tPAB** were calculated to be −5.21, −5.08, and −5.09 eV, respectively. From these HOMO values and the optical gap (E^{g}_{opt}) obtained from the absorption spectra, the LUMO energy levels were estimated to be −2.44, −2.34, and −2.36 eV, respectively (Table 1).

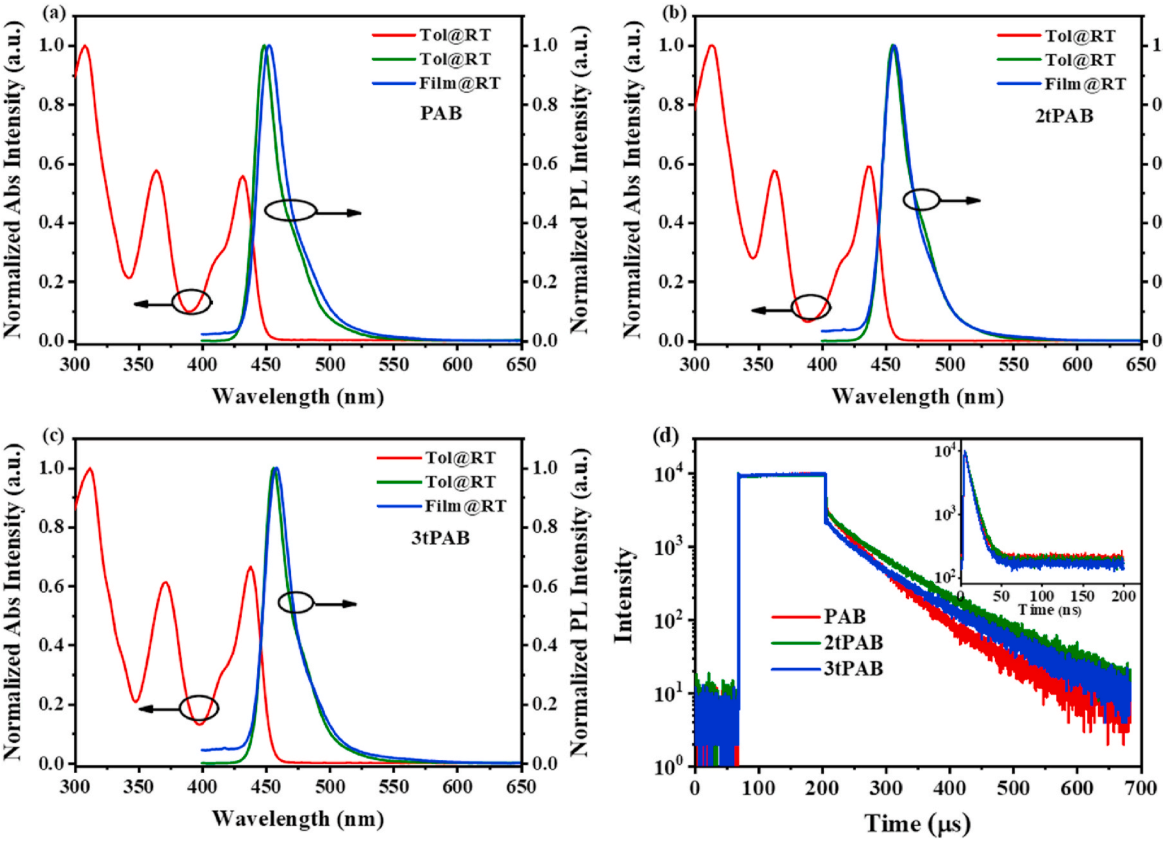

Fig. 4. UV–vis absorption (Abs, room temperature) and fluorescence (Fl, room temperature) spectra of (a) **PAB**, (b) **2tPAB** and (c) **3tPAB** in toluene (1.0×10^{-5} M) and fluorescence spectra of 3 wt % emitter in mCP. (d) Transient PL decay spectra of **PAB**/**2tPAB**/**3tPAB** doped into mCP films (3 wt%) at room temperature.

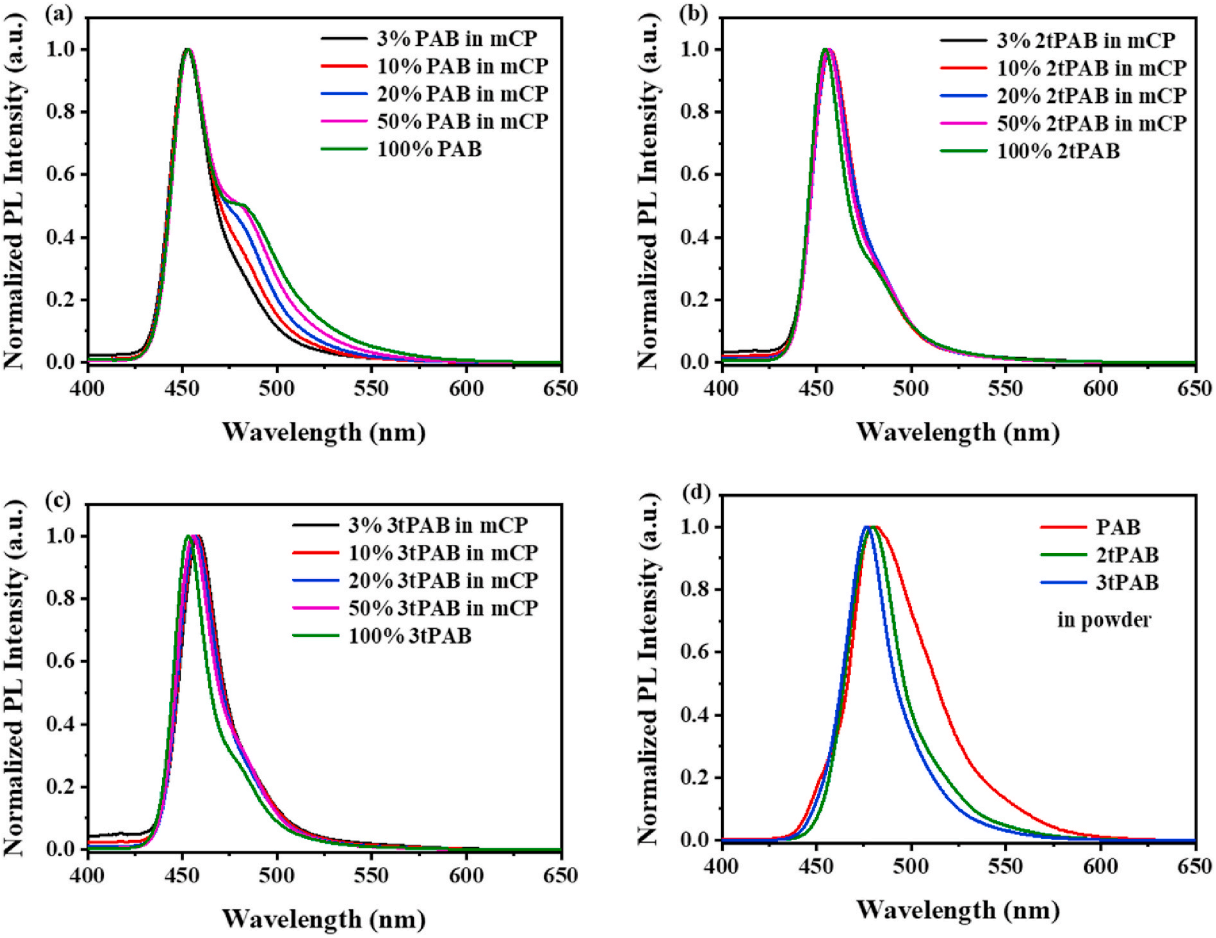

Fig. 5. The fluorescence spectra of (a) **PAB**, (b) **2tPAB** and (c) **3tPAB** in pure film and in mCP with different doping concentration. (d) The fluorescence spectra **PAB**, **2tPAB** and **3tPAB** in powder.

3.4. Photophysical properties

The photophysical properties of **PAB**, **2tPAB,** and **3tPAB** in solution and film were investigated (Fig. 4 and Table 1). The ultraviolet–visible (UV) absorption spectrum in toluene (1.0×10^{-5} M) revealed a strong absorption band at ~435 nm (maximum absorption wavelength), corresponding to the HOMO-LUMO transition [39]. Based on the onsets of absorption spectra, the optical gap (E^{g}_{opt}) of **PAB**, **2tPAB,** and **3tPAB** was calculated to be 2.77, 2.74, and 2.73 eV, respectively. **PAB** displayed a higher E^{g}_{opt} value than **2tPAB** and **3tPAB**, which was consistent with the results of theoretical calculations. The emission peaks of **PAB**, **2tPAB**, and **3tPAB** in cyclohexane/toluene/CH_2Cl_2 solutions were located at 438/449/458, 447/456/462, and 449/456/463 nm, respectively (Table 1 and Table S1). As analyzed in theoretical calculations, **PAB** exhibited more blue emission than **2tPAB**, **3tPAB** and DABNA-1 (462 nm in CH_2Cl_2 solutions) [38]. The introduction of *tert*-butyl unit into **2tPAB** and **3tPAB** increases donor strengths (electron donating nitrogen atom), further enhancing intensity of short-range intramolecular charge transfer and resulting in bathochromic shifts of emission. And from non-polar cyclohexane to strongly polar CH_2Cl_2, the shift of emission peak was 20 nm for **PAB**, 15 nm for **2tPAB**, and 14 nm for **3tPAB**, respectively. This indicated that peripheral *tert*-butyl units relieved the effect of solvent polarity on emission effectively. The FWHMs of **PAB**, **2tPAB**, and **3tPAB** in cyclohexane/toluene were 16/23, 18/26, and 18/23 nm, respectively. Even in the strongly polar solvents dichloromethane and *N,N*-dimethylformamide (Fig. S2), the FWHMs of the three compounds were still less than 28 nm. Such small FWHMs were among the best results in the TADF emitter with narrowband emission.

The fluorescence spectra of these three emitters doped in host mCP showed a slight redshift compared with that of in toluene (Fig. 4), which might be caused by interactions between the emitters and host. With the increase of doping concentration, **PAB** showed more obvious emission around 490 nm (Fig. 5). However, **2tPAB** and **3tPAB** exhibited little difference. The results demonstrated peripheral *tert*-butyl units suppressed intermolecular interactions and stacking. This can also be confirmed by their fluorescence spectrum in powder. As shown in Fig. 5d, **PAB** presented wider FWHM and a red-shift emission relative to **2tPAB** and **3tPAB**. The suppressed intermolecular interactions in **2tPAB** and **3tPAB** will help to suppress aggregation-induced emission quenching, thus reducing the energy loss through the non-radiative rotational relaxation channel and enhancing the luminescence performance. The absolute photoluminescence quantum yields (PLQY) in the doped film (3 wt% in mCP) of **PAB**, **2tPAB**, and **3tPAB** were measured to be 60.8%, 67.3%, and 74.7%, respectively, further demonstrating that the introduction of peripheral *tert*-butyl units of the **PAB** was beneficial to improve luminescent performance.

From the onsets of the low-temperature (77K) fluorescence and phosphorescence spectra (Fig. S3), the ΔE_{ST} value was calculated to be 0.06 eV for **PAB**, 0.08 eV for **2tPAB**, and 0.10 eV for **3tPAB**, respectively, indicating that the cladding of *tert*-butyl unit slightly increases the ΔE_{ST} of the emitter. To evaluate the TADF nature of **PAB**, **2tPAB**, and **3tPAB**, transient photoluminescence spectra of the doped film of 3 wt% emitters: mCP were measured (Fig. 4d). The prompt fluorescence lifetimes (τ_{PF}) were 7.9, 8.1, and 7.2 ns, and the delayed lifetimes (τ_{DF}) were 55.7, 76.6, and 74.2 μs for **PAB**, **2tPAB**, and **3tPAB**, respectively. According to the proportion of the integrated area of prompt and delayed

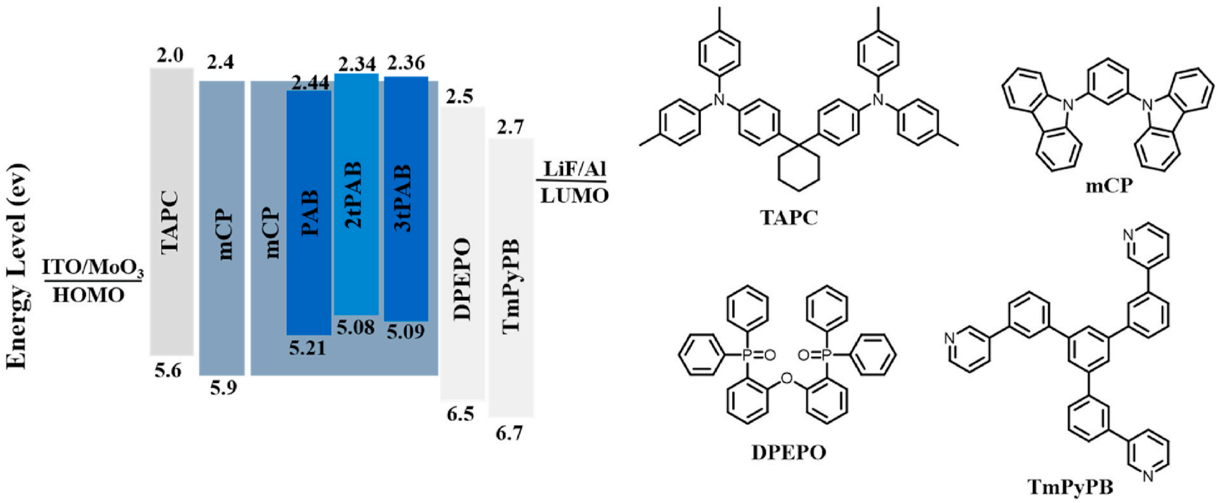

Fig. 6. The energy level diagram and molecular structures of the used materials in devices.

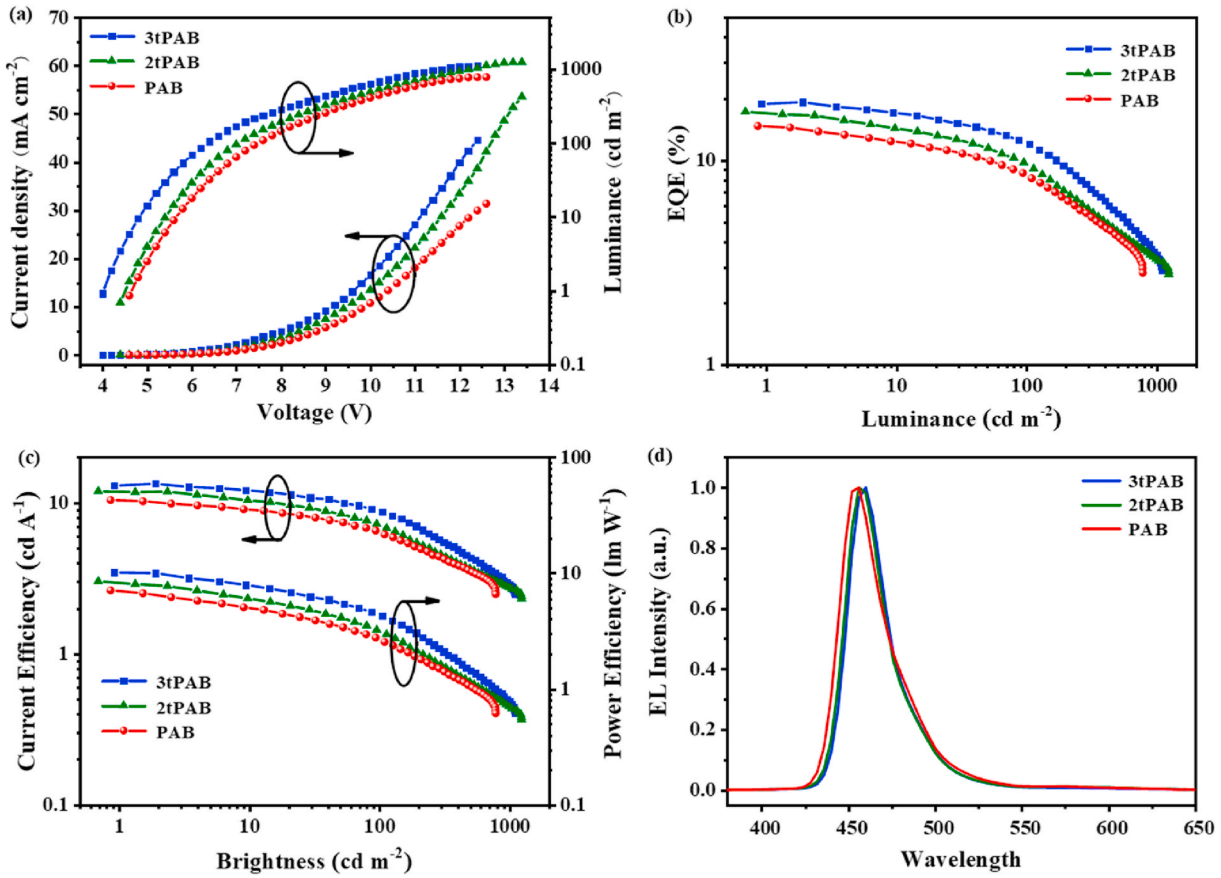

Fig. 7. (a) Current density-voltage-brightness (J-V-B) characteristics; (b) EQE-brightness curves; (c) current efficiency-brightness-power efficiency curves; (d) normalized EL spectra at 6 V.

fluorescence in the transient spectra to the total integrated area [40], the prompt and delayed fluorescence quantum yields, Φ_{PF} and Φ_{DF}, can be obtained (see Table S2). Furthermore, the rate constants for fluorescence (k_F), internal conversion (k_{IC}), intersystem crossing (k_{ISC}), and k_{RISC} were calculated using the reported method [10,41,42]. The results were presented in Table S2. The k_{RISC} of **PAB**, **2tPAB**, and **3tPAB** were 6.95×10^4 s^{-1}, 6.34×10^4 s^{-1}, and 5.74×10^4 s^{-1}, respectively. **PAB** exhibited a slightly higher k_{RISC} with 6.95×10^4 s^{-1} in the three compounds owing to the relatively small ΔE_{ST}.

3.5. Device performances

Given the narrow FWHM, high PLQY, and satisfactory TADF properties of **PAB**, **2tPAB**, and **3tPAB**, electroluminescence (EL) performance was evaluated. To suppress the effect of interactions between hosts and emitters on electroluminescence spectra, mCP with low polarity was selected as the host material. The optimized device configuration was ITO/MoO_3 (10 nm)/TAPC (60 nm)/mCP (5 nm)/mCP: 3 wt% emitter (20 nm)/DPEPO (15 nm)/TmPyPB (30 nm)/LiF (1 nm)/Al (100

Table 2
The EL performances of **PAB**, **2tPAB**, **3tPAB** and other narrowband blue TADF emitters in literature.

Compound	V_{on}[a] (V)	L_{max}[b] (cd m^{-2})	CE_{max}[b] (cd A^{-1})	PE_{max}[b] (lm W^{-1})	EQE_{max}[b] (%)	λ_{EL}[c]/FWHM[c] (nm)	CIE[d] (x, y)	Ref.
PAB	4.7	782	10.4	7.1	14.7	456/31	(0.145, 0.076)	This work
2tPAB	4.5	1241	11.8	8.0	16.8	456/27	(0.145, 0.076)	This work
3tPAB	4.1	1100	13.4	10.2	19.3	460/26	(0.141, 0.076)	This work
DABNA-1	–	<1000	10.6	8.3	13.5	459/28	(0.13, 0.09)	[38]
DABNA-2	–	<1000	21.1	15.1	20.2	467/28	(0.12, 0.13)	[38]
B2	–	<1000	16.7	13.8	18.3	460/37	(0.13, 0.11)	[43]
TBN-TPA	3.5	16593	40.2	30.0	32.1	474/27	(0.13, 0.19)	[30]
t-DABNA	–	–	32.6	33.6	31.4	466/31	(0.13, 0.15)	[29]
ν-DABNA	–	–	31.0	25.6	34.4	469/18	(0.12, 0.11)	[18]
TCz-BN	3.0	–	–	24.0	18.9	474/34	(0.13, 0.20)	[27]
ADBNA-Me-Tip	–	<1000	34.7	28.7	21.4	480/33	(0.11, 0.29)	[15]
QAO	–	<1000	26.2	31.6	19.4	468/39	(0.13, 0.18)	[24]
7-Ph-QAD	–	2944	28.8	28.2	18.7	472/34	(0.12, 0.14)	[25]
DiKTa	3.0	10385	–	–	14.7	465/39	(0.14,0.18)	[31]
QA-PCN	3.4	2760	22.6	–	16.9	473/30	(0.12, 0.18)	[26]
1	–	–	–	–	29.3	469/27	(0.12, 0.18)	[19]
DABNA-*N*P-TB	3.6	–	18.5	16.1	19.5	457/33	(0.14, 0.11)	[33]

[a] Voltage at 1 cd m^{-1} (V).
[b] Maximum luminance (cd m^{-1}); Maximum current efficiency (cd A^{-1}); Maximum power efficiency (lm W^{-1}); Maximum external quantum efficiency (%).
[c] The peak of the EL spectrum; Full width at half maximum of EL spectrum.
[d] Commission Internationale de l'Eclairage coordinates.

nm). The doping concentration, 3 wt%, was the optimized concentration. The energy level diagram and molecular structures of the used materials were shown in Fig. 6. MoO$_3$ and LiF were employed as hole and electron injection layer, respectively. 1,1-bis[(di-4-tolylamino) phenyl]cyclohexane (TAPC) and 3,30-(50-(3-(pyridin-3-yl)phenyl)-[1,10:30,100-terphenyl]-3300-diyl)dipyridine (TmPyPB) were used as hole and electron transporting layer, respectively. mCP and bis[2-(diphenylphosphino)phenyl] ether oxide (DPEPO) acted as exciton blocking layer.

The EL characteristics were shown in Fig. 7 and the key performance data were summarized in Table 2. The turn-on voltages of **PAB-**, **2tPAB-**, and **3tPAB**-based devices were 4.7, 4.5, and 4.1 V, respectively. The maximum luminance was 782, 1241, and 1100 cd m^{-2} for **PAB-**, **2tPAB-**, and **3tPAB**-based devices, respectively. **PAB-**, **2tPAB-**, and **3tPAB**-based devices exhibited deep-blue emission with peaks at 456, 456 and 460 nm and CIE coordinates of (0.145, 0.076), (0.145, 0.076) and (0.141, 0.076), respectively. The CIE coordinates of these devices met the NTSC blue-light standard of (0.14, 0.08). What's more, the FWHMs of **PAB**-, **2tPAB**-, and **3tPAB**-based devices were 31, 27, and 26 nm, respectively. The FWHMs of devices were decreased with the introduction of *tert*-butyl unit into emitter. This indicated that the introduction of *tert*-butyl unit into **2tPAB** and **3tPAB** decreased the intermolecular interactions, like hosts and emitters or emitter and emitter. However, the FWHMs of **PAB**, **2tPAB**, and **3tPAB** in toluene were 23, 26, and 23 nm, respectively. The FWHMs in toluene did not exhibit a decrease variation tendency, which might be due to the solvent polarity. As shown in Table S2, **PAB**, **2tPAB**, and **3tPAB** presented different variation tendency of FWHMs in different solvents. **PAB-**based device still exhibited more blue emission than that of DABNA-1-based device (Table 2) [34], demonstrating the availability of molecular design and device design strategy. The current efficiency (CE$_{max}$)/power efficiency (PE$_{max}$)/EQE$_{max}$ of **PAB-**, **2tPAB-**, and **3tPAB**-based devices were 10.4 cd A^{-1}/7.1 lm W^{-1}/14.7%, 11.8 cd A^{-1}/8.0 lm W^{-1}/16.8%, and 13.4 cd A^{-1}/10.2 lm W^{-1}/19.3%, respectively. It was found that the device efficiency was improved gradually from no periphery cladding to a full periphery cladding of emitter. The **3tPAB**-based device exhibited the highest efficiency among these devices. The better device performance of the **3tPAB**-based device was because of its higher PLQY. Specifically, to our knowledge, the external quantum efficiency with EQE$_{max}$ of 19.3% was the highest value that can satisfy the NTSC blue-light standard and narrowband emission in narrowband TADF OLEDs with single host to date (Table 2). These results demonstrated that a full periphery cladding with *tert*-butyl units in narrowband TADF emitter is important for the improvement of device performance.

4. Conclusion

In summary, we designed and synthesized three deep-blue narrowband TADF emitters with B-π-N structure (**PAB**, **2tPAB**, and **3tPAB**) by using the periphery cladding strategy. Although the introduction of peripheral *tert*-butyl group increased ΔE_{ST} of emitter and reduced reverse intersystem crossing rate, the intermolecular interactions and the aggregation-induced emission quenching were suppressed effectively. And the PLQY of TADF emitters was boosted without altering narrowband characteristics. Accordingly, **3tPAB** with a full periphery cladding exhibited a higher PLQY of 74.7%, which endowed it with superior device performance. By using mCP with low polarity as host, the **3tPAB**-based device exhibited the EQE$_{max}$ of 19.3%, CIE coordinates of (0.141, 0.076), and FWHMs of 26 nm, respectively. To our knowledge, this is the first report about narrowband TADF OLEDs with single host that can satisfy the NTSC blue-light standard. We believe that this work will encourage more endeavor to deep-blue high-efficiency narrowband OLEDs and promote the development of high resolution and wide color gamut for new-generation display technology.

Declaration of competing interest

The authors declare that they have no known competing financial interests or personal relationships that could have appeared to influence the work reported in this paper.

Acknowledgments

This research work was supported by the National Natural Science Foundation of China (62004074, 51727809), and Science and Technology Department of Hubei Province (2020BAA016, 2019AAA063). Wuhan Science and Technology Bureau (2019010701011406). Thanks to SCTS/CGCL HPCC of HUST for providing computing resources and technical support.

Appendix A. Supplementary data

Supplementary data to this article can be found online at https://doi.org/10.1016/j.orgel.2021.106275.

References

[1] D. Zhang, T. Huang, L. Duan, Emerging self-emissive technologies for flexible displays, Adv. Mater. 32 (2020) 1902391.

[2] Y. Wang, J.H. Yun, L. Wang, J.Y. Lee, High triplet energy hosts for blue organic light-emitting diodes, Adv. Funct. Mater. 31 (2020) 2008332.

[3] S.K. Jeon, H.L. Lee, K.S. Yook, J.Y. Lee, Recent progress of the lifetime of organic light-emitting diodes based on thermally activated delayed fluorescent material, Adv. Mater. 31 (2019) 1803524.

[4] J. Song, H. Lee, E.G. Jeong, K.C. Choi, S. Yoo, Organic light-emitting diodes: pushing toward the limits and beyond, Adv. Mater. 32 (2020) 1907539.

[5] A. Khan, X. Tang, C. Zhong, Q. Wang, S.-Y. Yang, F.-C. Kong, S. Yuan, A.S. D. Sandanayaka, C. Adachi, Z.-Q. Jiang, L.-S. Liao, Intramolecular-locked high efficiency ultrapure violet-blue (CIE-y $<$0.046) thermally activated delayed fluorescence emitters exhibiting amplified spontaneous emission, Adv. Funct. Mater. 31 (2021) 2009488.

[6] X. Yang, X. Xu, G. Zhou, Recent advances of the emitters for high performance deep-blue organic light-emitting diodes, J. Mater. Chem. C 3 (2015) 913–944.

[7] C. Yao, Y. Yu, X. Yang, H. Zhang, Z. Huang, X. Xu, G. Zhou, L. Yue, Z. Wu, Effective blocking of the molecular aggregation of novel truxene-based emitters with spirobifluorene and electron-donating moieties for furnishing highly efficient non-doped blue-emitting OLEDs, J. Mater. Chem. C 3 (2015) 5783–5794.

[8] W. Liu, S. Ying, R. Guo, X. Qiao, P. Leng, Q. Zhang, Y. Wang, D. Ma, L. Wang, Nondoped blue fluorescent organic light-emitting diodes based on benzonitrile-anthracene derivative with 10.06% external quantum efficiency and low efficiency roll-off, J. Mater. Chem. C 7 (2019) 1014–1021.

[9] H. Uoyama, K. Goushi, K. Shizu, H. Nomura, C. Adachi, Highly efficient organic light-emitting diodes from delayed fluorescence, Nature 492 (2012) 234–238.

[10] Q. Zhang, H. Kuwabara, J. William J. Potscavage, S. Huang, Y. Hatae, T. Shibata, C. Adachi, Anthraquinone-based intramolecular charge-transfer compounds: computational molecular design, thermally activated delayed fluorescence, and highly efficient red electroluminescence, J. Am. Chem. Soc. 136 (2014) 18070–18081.

[11] L. Cao, K. Klimes, Y. Ji, T. Fleetham, J. Li, Efficient and stable organic light-emitting devices employing phosphorescent molecular aggregates, Nat. Photonics 15 (2021) 230–237.

[12] X. Lv, Y. Wang, N. Li, X. Cao, G. Xie, H. Huang, C. Zhong, L. Wang, C. Yang, Regulating the photophysical properties of highly twisted TADF emitters by concurrent through-space/-bond charge transfer, Chem. Eng. J. 402 (2020) 126173.

[13] V.V. Patil, K.H. Lee, J.Y. Lee, Dibenzo[c,g]indolo[3,2,1-jk]carbazole as a new chromophore for blue organic light-emitting diodes, J. Mater. Chem. C 7 (2019) 14301–14305.

[14] D. Song, Y. Yu, L. Yue, D. Zhong, Y. Zhang, X. Yang, Y. Sun, G. Zhou, Z. Wu, Asymmetric thermally activated delayed fluorescence (TADF) emitters with 5,9-dioxa-13bboranaphtho[3,2,1-de]anthracene (OBA) as the acceptor and highly efficient blue-emitting OLEDs, J. Mater. Chem. C 7 (2019) 11953–11963.

[15] S. Oda, B. Kawakami, R. Kawasumi, R. Okita, T. Hatakeyama, Multiple resonance effect-induced sky-blue thermally activated delayed fluorescence with a narrow emission band, Org. Lett. 21 (2019) 9311–9314.

[16] H. Hirai, K. Nakajima, S. Nakatsuka, K. Shiren, J. Ni, S. Nomura, T. Ikuta, T. Hatakeyama, One-step borylation of 1,3-Diaryloxybenzenes towards efficient materials for organic light-emitting diodes, Angew. Chem. Int. Ed. 54 (2015) 13581–13585.

[17] S. Madayanad Suresh, D. Hall, D. Beljonne, Y. Olivier, E. Zysman-Colman, Multiresonant thermally activated delayed fluorescence emitters based on heteroatom-doped nanographenes: recent advances and prospects for organic light-emitting diodes, Adv. Funct. Mater. 30 (2020) 1908677.

[18] Y. Kondo, K. Yoshiura, S. Kitera, H. Nishi, S. Oda, H. Gotoh, Y. Sasada, M. Yanai, T. Hatakeyama, Narrowband deep-blue organic light-emitting diode featuring an organoboron-based emitter, Nat. Photonics 13 (2019) 678–682.

[19] M. Yang, I.S. Park, T. Yasuda, Full-color, narrowband, and high-efficiency electroluminescence from boron and carbazole embedded polycyclic heteroaromatics, J. Am. Chem. Soc. 142 (2020) 19468–19472.

[20] X. Cai, S.-J. Su, Marching toward highly efficient, pure-blue, and stable thermally activated delayed fluorescent organic light-emitting diodes, Adv. Funct. Mater. 28 (2018) 1802558.

[21] J.-M. Teng, Y.-F. Wang, C.-F. Chen, Recent progress of narrowband TADF emitters and their applications in OLEDs, J. Mater. Chem. C 8 (2020) 11340–11353.

[22] Z. Xu, B.Z. Tang, Y. Wang, D. Ma, Recent advances in high performance blue organic light-emitting diodes based on fluorescence emitters, J. Mater. Chem. C 8 (2020) 2614–2642.

[23] D. Chen, W. Li, L. Gan, Z. Wang, M. Li, S.-J. Su, Non-noble-metal-based organic emitters for OLED applications, Mater. Sci. Eng. R Rep. 142 (2020) 100581.

[24] Y. Yuan, X. Tang, X.-Y. Du, Y. Hu, Y.-J. Yu, Z.-Q. Jiang, L.-S. Liao, S.-T. Lee, The design of fused amine/carbonyl system for efficient thermally activated delayed fluorescence: novel multiple resonance core and electron acceptor, Adv. Opt. Mater. 7 (2019) 1801536.

[25] X. Li, Y.-Z. Shi, K. Wang, M. Zhang, C.-J. Zheng, D.-M. Sun, G.-L. Dai, X.-C. Fan, D.-Q. Wang, W. Liu, Y.-Q. Li, J. Yu, X.-M. Ou, C. Adachi, X.-H. Zhang, Thermally activated delayed fluorescence carbonyl derivatives for organic light-emitting diodes with extremely narrow full width at half-maximum, ACS Appl. Mater. Interfaces 11 (2019) 13472–13480.

[26] X. Qiu, G. Tian, C. Lin, Y. Pan, X. Ye, B. Wang, D. Ma, D. Hu, Y. Luo, Y. Ma, Narrowband emission from organic fluorescent emitters with dominant low-frequency vibronic coupling, Adv. Opt. Mater. 9 (2020) 2001845.

[27] Y. Zhang, D. Zhang, J. Wei, Z. Liu, Y. Lu, L. Duan, Multi-resonance induced thermally activated delayed fluorophores for narrowband green OLEDs, Angew. Chem. Int. Ed. 58 (2019) 16912–16917.

[28] Y. Xu, Z. Cheng, Z. Li, B. Liang, J. Wang, J. Wei, Z. Zhang, Y. Wang, Molecular-structure and device-configuration optimizations toward highly efficient green electroluminescence with narrowband emission and high color purity, Adv. Opt. Mater. 8 (2020) 1902142.

[29] S.H. Han, J.H. Jeong, J.W. Yoo, J.Y. Lee, Ideal blue thermally activated delayed fluorescence emission assisted by a thermally activated delayed fluorescence assistant dopant through a fast reverse intersystem crossing mediated cascade energy transfer process, J. Mater. Chem. C 7 (2019) 3082–3089.

[30] X. Liang, Z.-P. Yan, H.-B. Han, Z.-G. Wu, Y.-X. Zheng, H. Meng, J.-L. Zuo, W. Huang, Peripheral amplification of multi-resonance induced thermally activated delayed fluorescence for highly efficient OLEDs, Angew. Chem. Int. Ed. 57 (2018) 11316–11320.

[31] D. Hall, S.M. Suresh, P.L. dos Santos, E. Duda, S. Bagnich, A. Pershin, P. Rajamalli, D.B. Cordes, A.M.Z. Slawin, D. Beljonne, A. Köhler, I.D.W. Samuel, Y. Olivier, E. Zysman-Colman, Improving processability and efficiency of resonant TADF emitters: a design strategy, Adv. Opt. Mater. 8 (2020) 1901627.

[32] D. Sun, S.M. Suresh, D. Hall, M. Zhang, C. Si, D.B. Cordes, A.M.Z. Slawin, Y. Olivier, X. Zhang, E. Zysman-Colman, The design of an extended multiple resonance TADF emitter based on a polycyclic amine/carbonyl system, Mater. Chem. Front. 4 (2020) 2018–2022.

[33] S. Oda, W. Kumano, T. Hama, R. Kawasumi, K. Yoshiura, T. Hatakeyama, Carbazole-based DABNA analogs as highly efficient thermally activated delayed fluorescence materials for narrowband organic light-emitting diodes, Angew. Chem. Int. Ed. 60 (2021) 2882–2886.

[34] J.A. Knöller, G. Meng, X. Wang, D. Hall, A. Pershin, D. Beljonne, Y. Olivier, S. Laschat, E. Zysman-Colman, S. Wang, Intramolecular borylation via sequential B-Mes bond cleavage for the divergent synthesis of B,N,B-doped Benzo[4] helicenes, Angew. Chem. Int. Ed. 59 (2020) 3156–3160.

[35] Z. Cheng, Z. Li, Y. Xu, J. Liang, C. Lin, J. Wei, Y. Wang, Achieving efficient blue delayed electrofluorescence by shielding acceptors with carbazole units, ACS Appl. Mater. Interfaces 11 (2019) 28096–28105.

[36] J. Lee, N. Aizawa, M. Numata, C. Adachi, T. Yasuda, Versatile molecular functionalization for inhibiting concentration quenching of thermally activated delayed fluorescence, Adv. Mater. 29 (2017) 1604856.

[37] D. Zhang, M. Cai, Y. Zhang, D. Zhang, L. Duan, Sterically shielded blue thermally activated delayed fluorescence emitters with improved efficiency and stability, Mater. Horiz. 3 (2016) 145–151.

[38] T. Hatakeyama, K. Shiren, K. Nakajima, S. Nomura, S. Nakatsuka, K. Kinoshita, J. Ni, Y. Ono, T. Ikuta, Ultrapure blue thermally activated delayed fluorescence molecules: efficient HOMO–LUMO separation by the multiple resonance effect, Adv. Mater. 28 (2016) 2777–2781.

[39] N. Ikeda, S. Oda, R. Matsumoto, M. Yoshioka, D. Fukushima, K. Yoshiura, N. Yasuda, T. Hatakeyama, Solution-processable pure green thermally activated delayed fluorescence emitter based on the multiple resonance effect, Adv. Mater. 32 (2020) 2004072.

[40] D. Zhang, X. Song, A.J. Gillett, B.H. Drummond, S.T.E. Jones, G. Li, H. He, M. Cai, D. Credgington, L. Duan, Efficient and stable deep-blue fluorescent organic light-emitting diodes employing a sensitizer with fast triplet upconversion, Adv. Mater. 32 (2020) 1908355.

[41] K. Masui, H. Nakanotani, C. Adachi, Analysis of exciton annihilation in high-efficiency sky-blue organic light-emitting diodes with thermally activated delayed fluorescence, Org. Electron. 14 (2013) 2721–2726.

[42] H. Kaji, H. Suzuki, T. Fukushima, K. Shizu, K. Suzuki, S. Kubo, T. Komino, H. Oiwa, F. Suzuki, A. Wakamiya, Y. Murata, C. Adachi, Purely organic electroluminescent material realizing 100% conversion from electricity to light, Nat. Commun. 6 (2015) 8476.

[43] K. Matsui, S. Oda, K. Yoshiura, K. Nakajima, N. Yasuda, T. Hatakeyama, One-shot multiple borylation toward BN-doped nanographenes, J. Am. Chem. Soc. 140 (2018) 1195–1198.